Photovoltaic power plant source measurement system for fault detection

1st Matěj Turinský
Department of Control and Instrumentation
Brno University of Technology
Brno, Czech Republic
0009-0000-8748-8384

***Abstract*—This paper describes a novel system for the monitoring of the string segment of a photovoltaic (PV) power plant. The design of the monitoring device is intended for future use in the detection of arc faults and the tracking of long-term degradation of the solar panels. The primary benefits of such a system are expected to be enhanced safety and simplified maintenance for existing PV installations. The monitoring system is based on the Texas Instruments C2000 platform, which performs all measurements and also acts as Modbus RTU server to propagate the results. To facilitate the installation on existing PV power plants, a G3-PLC modem has been used to transfer measurements to a data acquisition system without any need for extra communication wires. A prototype of the proposed device has been constructed and demonstrated to function under laboratory conditions.**

***Index Terms*—Photovoltaic, data acquisition system, maintenance, solar panel degradation, safety, arc faults**

I. Introduction

According to the forecasts conducted by ČEPS, it is expected that the installed capacity of PV power plants will increase from 5.67GW to 10.71GW between the years 2025 and 2030 [1]. This represents the most significant increase in installed capacity since 2020, thus establishing PV power plants as the most represented renewable power sources in the Czech Republic. This suggests that demands on safety, particularly fire safety, will increase, along with demands on maintenance to prevent potential losses.

The most critical risk associated with the PV power plant opperation is the occurance of the arc faults, which can result in fires if they occur repeatedly. Arc faults can be categorised into two primary types: serial and parallel [2].

Serial arc typically forms at the points with increased contact resistance, electrical field strength, humidity and temperature. Therefore, mechanically stressed, corroded or loose contacts and connectors are the most common causes of serial arc faults.

In contrast, parallel arc occurs when two conductors with different potentials come into contact. There are many combinations of such conductors in PV power plants, but typical examples include contact of positive and negative conductors within string, in between two strings and between conductor and ground. This means that a parallel arc is essentially a short circuit, but because PV cells are high internal impedance sources, the current increases to a maximum of 1.5 times the rated current. It is also true that parallel arcs highly depend on the condition of the conductor insulation.

Both types of arc fault are dangerous from a fire safety point of view, but they behave differently when string circuit is disconnected. If the circuit breaker has sufficient DC voltage rating, the serial arc will be interrupted when the circuit is opened, but if this happens during parallel arc fault, the load will be disconnected from the panels or the string and the arc may become even stronger. For this reason, standard arc fault circuit interrupters (AFCI) can cause problems for PV installations [2].

In order to ensure an effective long-term maintenance of the PV power plant, it is important to closely monitor the power trends. The reason for this is, that they serve as reliable indicators for distinguishing between short-term failures, such as panel shading and associated PV cell overheating, and long-term failures related to panel ageing, including panel delamination, discolouration, potential-induced degradation (PID) effect and corrosion [3] [4].

Finally, when discussing PV power plant maintenance, it is necessary to monitor the state of the additional PV installation components, including junction boxes, optimizers, maximum power point trackers (MPPT) and inverters. However, the most prone to failure additional components, which are part of each solar panel, are blocking and bypass schottky diodes connected in series with string and in parallel with panel or part of it respectively [5].

The subsequent sections detail the design of a prototype data acquisition system that complies with the previously mentioned criteria in terms of safety and maintenance needs. In Section II-A, the selection of measured quantities and the measurement method itself are described. The following Section II-B describes the selection of hardware and software implementation for the realisation of necessary measurements and communication of results via Modbus RTU protocol.

The author would like to thank to his supervisor Petr Fiedler for support and suggestions during the preparation of the paper, and to company ModemTec s.r.o., which participated in the development of the prototype measurement system.

II. Methods

The measurement and fault detection systems for PV power plants can be divided into two groups based on the type of processed data.

The first type of processed data are images in the visible or infrared spectrum. Examples of such images can be seen on Figure 1. While imaging methods are beneficial for localising faults, they are not suitable for fault detection due to the fact that they monitor secondary manifestations of faults, such as cell overheating, and also are still more expensive in comparison with sensing electrical quantities.

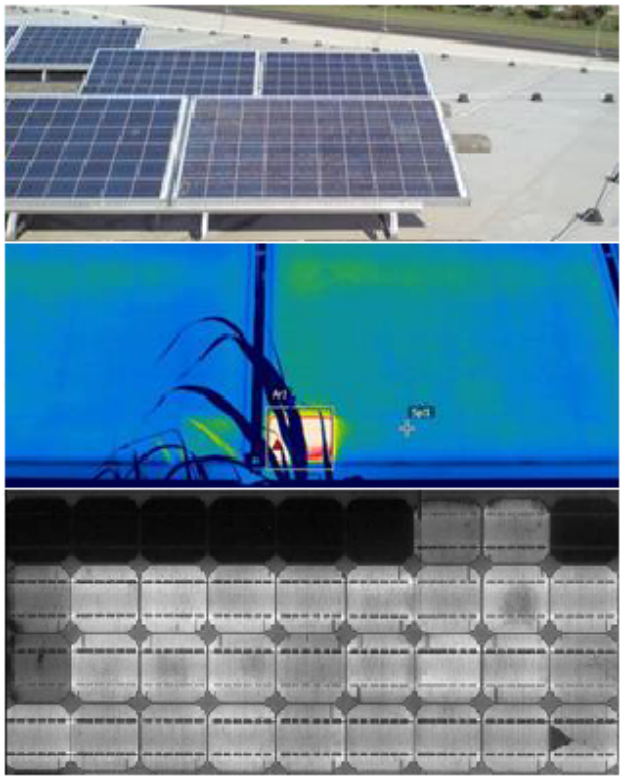

Fig. 1. Visible, infrared and electroluminescence solar panel imaging [6]

The second type of processed data are electrical quantities, such as current and voltage of the panel or string, and non-electrical quantities, including ambient and panel temperature, solar irradiance or humidity. This type of data direcly indicates the state of the PV installation, with particular emphasis on the solar panels.

A. Measured quantities

As previously mentioned in the introduction, the most critical measurements should be related to arc fault detection. The most convenient way to do this is to process the panel or string current and voltage spectra. The arc fault event changes the nominal power spectra in frequency bands ranging from 40 to 100 kHz [7].

For the purpose of long-term maintenance, the 'Weahter-corrected performance ratio' PR_{corr} presented in [8] is a suitable indicator, which is computed using the following formula:

$$PR_{corr} = \frac{\sum_k P_{out,k} \cdot \tau_k}{\sum_k \frac{(1+\gamma \cdot (T_{mod,k}-25)) \cdot P_0 \cdot G_{i,k} \cdot \tau_k}{G_{i,ref}}} \quad (1)$$

Where $P_{out,k}$ represents the power in the AC power plant part in step k in kilowatts, τ_k step duration in hours, γ relative maximum power temperature coefficient, $T_{mod,k}$ temperature of PV cell or panel in step k in degrees Celsius, P_0 installed power in the DC power plant part in kilowatts, $G_{i,k}$ solar irradiance in step k and $G_{i,ref}$ solar irradiance expected for power P_0 both in kilowatts per square meter.

All the measured quantities necessary to fulfil both arc fault and long-term monitoring are listed in Table I, in conjunction with the relevant constraints for each measurement.

TABLE I
Quantities measured by fault detection system

Quantity (unit)	***Constrains***
Current (A)	Range up to 10 A, sampling frequency at least 200 kHz
Voltage (V)	Range adjustment from 1.5 kV, surge protection 8 kV (CAT III)
Solar irradiance (Wm^{-2})	Similar spectral response with PV cells
Ambient temperature (°C)	Range according to ambient temperatures
Panel temperature (°C)	Range up to 120°C
Current time (s)	Unix time format support
Differential current (A)	Minimum 6 mA leakage current detection

B. Prototype design

The measurement system is designed to be installed at the point where the string connects to the power plant main bus. This wiring configuration provides an acceptable compromise between the accuracy of panel condition estimation and the number of measuring points, while taking advantage of the PV power plant topology for easy communication via G3-PLC over the main bus.

The prototype itself is built around the LaunchXL-F28069M development kit [9] containing TMS320F28069 microcontroller, which is optimised for real-time applications such as feedback control and online signal processing. For the purpose of string current measurement, an ACS37002 current sensor [10] is utilised and connected to the first ADC channel of the microcontroller. The second ADC channel is connected via a 1:470 voltage divider with a surge protection circuit and a voltage follower with small input current, for the purpose of string voltage measurement. Simultaneous sampling is used for the string current and voltage measurements, so that it is possible to compute string power without any time shift suppression needed. After that, the second ADC channel is used to sample a voltage from a photoresistor-based solar irradiance sensor [11]. Both ADC channels are equipped with their own sample and hold circuitry, which is connected via

analog multiplexer to 12-bit successive approximation ADC.

Finally, temperature measurements are taken using a TCN75A digital temperature sensor [12], one placed in the open air and one on the back of the solar panel, connected to the microcontroller via an I^2C bus, and leakage current detection is performed by T60404-N4641-X900 differential current sensor [13], whose trip contact is connected to the digital input of the microcontroller.

The overall wiring of the measurement system is then shown by the block diagram in Figure 2.

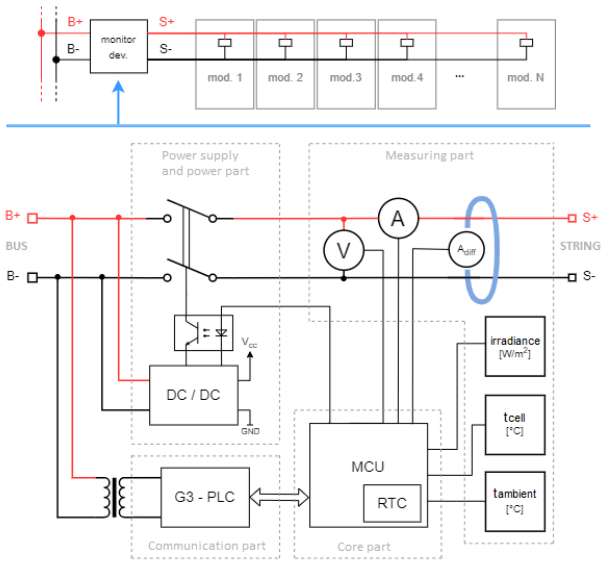

Fig. 2. Measurement system block diagram

C. Software implementation

The microcontroller utilised is equiped with two cores and so the software is also divided into two parts. The first part of the program is dedicated to the CLA core, which is optimised to accelerate the real-time calculations. For this reason, the CLA core is used for process data from the ADC. Program for the CLA core is divided into so called tasks, which are event-driven routines with a priority order of execution. The higher priority Task 1 is triggered by the start of AD conversion of the string current and voltage, which in turn is triggered by the timer overflow event that occurs every 2 μs. The lower priority Task 2 is then triggered by the conversion of the voltage on the photoresistor-based solar irradiance sensor. This Task is also triggered by the timer overflow event, but with a 1 ms period instead. The program for both CLA tasks is then described by the Algorithm 1.

The arc detection filters used in Algorithm 1 are 8^{th} order Butterworth type IIR with frequency response shown in Figure 3, valid for the 500 kHz sampling frequency. The selection of the Butterworth filter was driven by its flat passband response, while the order of the filter was determined by the capabilities of the MCU. The filter

Algorithm 1 – Program for the CLA core

Task 1:

$\mathbf{sc}_{1:N} \leftarrow \mathbf{sc}_{0:N-1}$

$\mathbf{sc}_0 = (\mathrm{ADC}^{\mathrm{current}} \cdot \mathrm{Scale}^{\mathrm{current}}) + \mathrm{Offset}^{\mathrm{current}}$

$\mathrm{sc}_{\mathrm{AVG}} = \frac{1}{N} \sum_{i=0}^{N} \mathbf{sc}_i$

$\mathbf{temp} \leftarrow []$

for i $\leftarrow$ 0 : k **do**

  $\mathbf{temp}_i = \sum_{j=0}^{M} \mathbf{FN}_{i,j} \cdot \mathbf{sc}_j + \mathbf{FD}_{i,j} \cdot \mathbf{FC}_{i,j}$

  $\mathbf{af}_i = \mathbf{temp}_i \geq \mathrm{Treshold}^{\mathrm{arc\text{-}fault}}$

  $\mathbf{FC}_{i,\,1:M} \leftarrow \mathbf{FC}_{i,\,0:M-1}$

  $\mathbf{FC}_{i,\,0} \leftarrow \mathbf{temp}_i$

end for

$\mathbf{sv}_{1:N} \leftarrow \mathbf{sv}_{0:N-1}$

$\mathbf{sv}_0 = (\mathrm{ADC}^{\mathrm{voltage}} \cdot \mathrm{Scale}^{\mathrm{voltage}}) + \mathrm{Offset}^{\mathrm{voltage}}$

$\mathrm{sv}_{\mathrm{AVG}} = \frac{1}{N} \sum_{i=0}^{N} \mathbf{sv}_i$

return $\leftarrow [\mathrm{sc}_{\mathrm{AVG}}, \mathrm{sv}_{\mathrm{AVG}}, \mathbf{af}, \mathbf{sc}, \mathbf{sv}]$

Task 2:

temp $\leftarrow []$

$\mathrm{temp} = (\mathrm{ADC}^{\mathrm{resistance}} \cdot \mathrm{Scale}^{\mathrm{resistance}}) + \mathrm{Offset}^{\mathrm{resistance}}$

$\mathbf{ir}_{1:N} \leftarrow \mathbf{ir}_{0:N-1}$

$\mathbf{ir}_0 = \mathrm{Scale}^{\mathrm{irradiance}} \cdot (\mathrm{temp})^{\mathrm{Exponent}^{\mathrm{irradiance}}}$

$\mathrm{ir}_{\mathrm{AVG}} = \frac{1}{N} \sum_{i=0}^{N} \mathbf{ir}_i$

return $\leftarrow [\mathrm{ir}_{\mathrm{AVG}}]$

Legend:

sc ... *N* previous string current values
FC ... *M* previous filtered current values from *k* filters
FN ... *M* numerator IIR coefficients from *k* filters
FD ... *M* denumerator IIR coefficients from *k* filters
af ... *M* arc fault detection boolen flags
sv ... *N* previous string voltage values
ir ... *N* previous solar irradiance values

design process MATLAB script that generates the header file containing the filter coefficients for CLA Task 1 algorithm has been written.

The actual conversion of the string current and voltage values from the ADC readings is expected to be linear, but depends on the gain of the input circuitry and is therefore adjustable.

For the conversion between resistance and solar irradiance the conversion characteristic, shown on a logarithmic scale in Figure 4, obtained from reference measurements interleaved with the least squares method is used. This characteristic applies to the GL5528 photoresistor [14] used in the protype measurement system.

The second core of the TMS320F28069 is mainly used as a data concentrator and Modbus RTU server. It periodically checks arc fault flags from the CLA core to determine if broadband noise generated by arc faults is present. It then reads the I2C temperature sensors at addresses

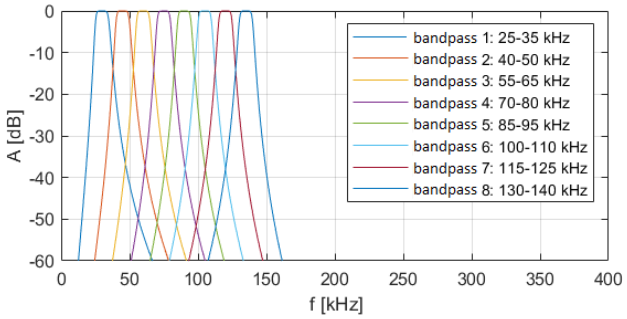

Fig. 3. Frequency response of arc detection filters

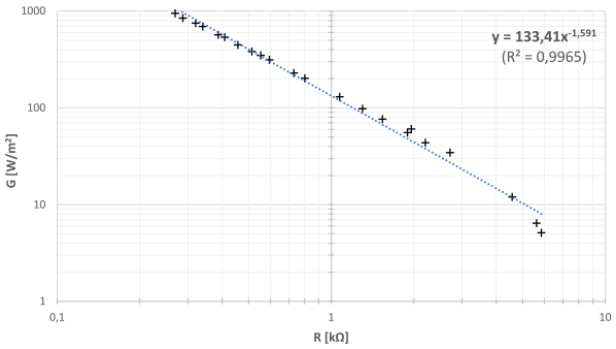

Fig. 4. Dependace of solar irradiance on photoresistor resistance

0x49 for ambient temperature and 0x4A for solar panel temperature, and the differential current sensor contact with a GPIO configured as a digital input. These measurements are then stored in the appropriate Modbus registers listed in Table II. The Modbus RTU server implementation is based on the nanoModbus library [15], which is freely distributed under the MIT licence.

TABLE II
MEASUREMENT SYSTEM MODBUS REGISTER MAP

Modbus register(s)	***Data type [bitlength]***	***Description***
1	bitfield [16b]	Configuration register (*Reserved*)
10001	bitfield [16b]	Status register (*Reserved*)
10002	bitfield [16b]	Leakage current detection (LSB)
30001-30002	float [32b]	String voltage (V)
30003-30004	float [32b]	String current (A)
30005-30006	float [32b]	String power (W)
30007-30008	float [32b]	Solar irradiance (Wm^{-2})
30009-30010	float [32b]	Panel temperature (°C)
30011-30012	float [32b]	Ambient temperature (°C)
40001-40004	unsigned [64b]	Processor time in Unix format (s)
40005-40006	float [32b]	String energy (J)
40007	unsigned [16b]	Arc fault occurance counter

III. RESULTS

The communication capabilities of the prototype have been verified under laboratory conditions in a simple power line communication network using two MT49S G3-PLC modems, one connected to the LaunchXL-F28069M development board via the UART interface and the other to the computer via the USB-RS485 converter. The test setup is shown in Figure 5.

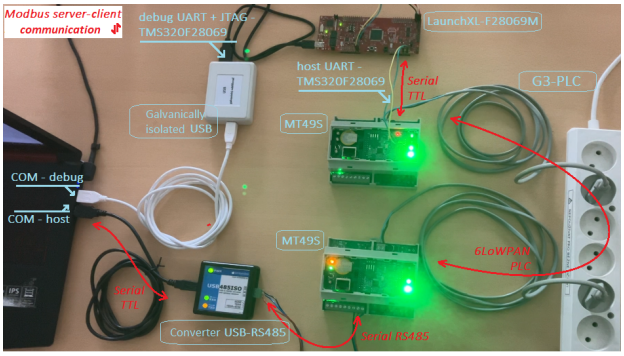

Fig. 5. Modbus RTU server test setup

The test measurements were then performed on a small PV power plant with six solar panels and a Huawei SUN2000 inverter, with a main focus on arc fault detection. Frequency and time domain plots of arc onset are shown in Figure 6 in conjunction with a sliding spark gap device used for the measurements. Subsequently, the filtration process of the retrieved current measurements, as outlined in Algorithm 1, resulted in the following results. It was determined that the arc fault has the highest impact on the frequency range between 25 and 50 kHz. For frequencies from 50 to 80 kHz is the impact too minor to be detected with simple tresholding but is still recognizable. The impact of the remaining higher frequency bands was found to be negligible, as illustrated in the filtered measurement in Figure 7.

IV. CONCLUSION

This paper presents a measurement system designed for a PV power plant. The primary purpose of this system is to detect short-term failures such as arc faults as well as long-term failures related to solar panel ageing. A prototype based on LaunchXL-F28069M has been developed and tested under laboratory conditions. Preliminary tests prove that the proposed measurement system can improve the safety of PV power plants and can even be installed in existing PV installations being a particularly important consideration in the context of increasingly stricter regulations.

Subsequent to these preliminary tests, it is imperative to conduct further testing in a field setting to collect substantial data, which will contribute to enhancement of the arc fault detection and the proper identification of long-term failures.

ACKNOWLEDGMENT

The research was funded from the grant No. FEKT-S-23-8451 – *"Research on advanced methods and technologies in cybernetics, robotics, artificial intelligence, automation and measurement"*, integrated with the Internal science fund of Brno University of Technology.

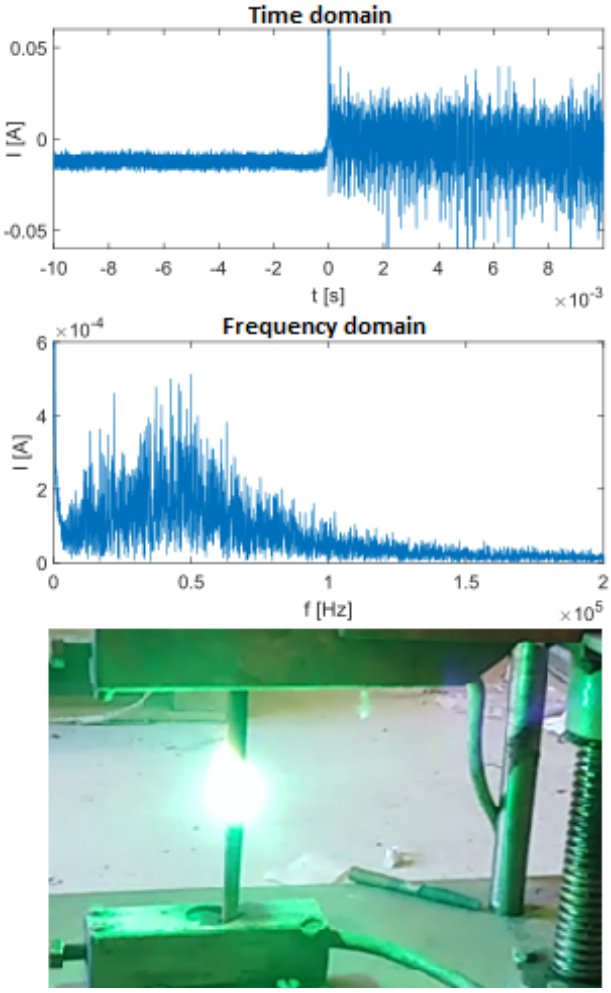

Fig. 6. Arc fault detection test measurements

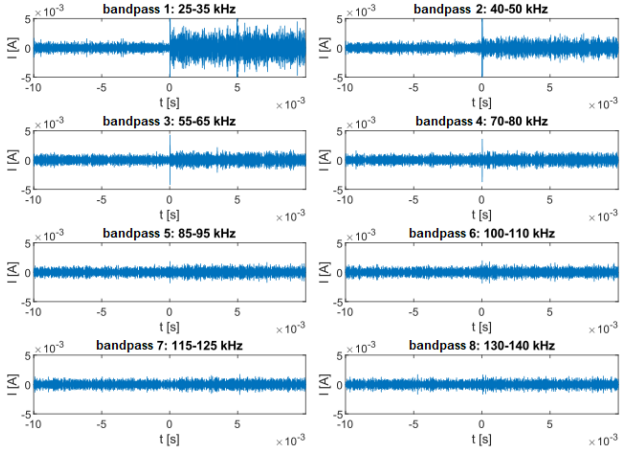

Fig. 7. Arc fault filtered current measurement

References

[1] ČEPS - Odbor 18320 Systémové analýzy ES, "Hodnocení zdrojové přiměřenosti ES ČR do roku 2040 (MAF CZ 2023)," https://www.ceps.cz/cs/zdrojova-primerenost, October 2024, [Accessed: 2025-01-27].

[2] J. Johnson, M. Montoya, S. McCalmont, G. Katzir, F. Fuks, J. Earle, A. Fresquez, S. Gonzalez, and J. Granata, "Differentiating series and parallel photovoltaic arc-faults," in *2012 38th IEEE Photovoltaic Specialists Conference*. IEEE, 2012, pp. 720–726.

[3] K. M. Sundaram, S. Padmanaban, J. B. Holm-Nielsen, and P. Pandiyan, *Photovoltaic Systems: Artificial Intelligence-based Fault Diagnosis and Predictive Maintenance*. CRC Press, 2022.

[4] L. Martin, "Pokles výkonu fotovoltaických elektráren v důsledku vysokonapěťového stresu." https://oze.tzb-info.cz/fotovoltaika/12260-pokles-vykonu-fotovoltaickychelektraren-v-dusledku-vysokonapetoveho-stresu, January 2015, [Accessed: 2025-01-28].

[5] Y.-Y. Hong and R. A. Pula, "Methods of photovoltaic fault detection and classification: A review," *Energy Reports*, vol. 8, pp. 5898–5929, 2022.

[6] U. Jahn, M. Herz, M. Köntges, D. Parlevliet, M. Paggi, I. Tsanakas, J. Stein, K. A. Berger, S. Ranta, R. H. French *et al.*, *Review on infrared and electroluminescence imaging for PV field applications: International Energy Agency Photovoltaic Power Systems Programme*. International Energy Agency, 2018.

[7] B. Novak, "Implementing arc detection in solar applications: achieving compliance with the new ul 1699b standard," *Texas Instruments*, 2012.

[8] T. Dierauf, A. Growitz, S. Kurtz, J. L. B. Cruz, E. Riley, and C. Hansen, "Weather-corrected performance ratio," National Renewable Energy Lab.(NREL), Golden, CO (United States), Tech. Rep., 2013.

[9] Texas Instruments, *TMS320F2806x Real-Time Microcontrollers*, SPRS698J, November 2010, [Revised Sept. 2021].

[10] Allegro microsystems, *ASC37002 400 kHz, High Accuracy Current Sensor*, ASC37002-DS, August 2024, [Revision 9].

[11] R. C. de Barros, J. M. S. Callegari, D. do Carmo Mendonça, W. C. S. Amorim, M. P. Silva, and H. A. Pereira, "Low-cost solar irradiance meter using LDR sensors," in *2018 13th IEEE International Conference on Industry Applications (INDUSCON)*. IEEE, 2018, pp. 72–79.

[12] Microchip Technology, *TCN75A 2-Wire Serial Temperature Sensor*, DS21935D, September 2010, [Revision D].

[13] VACUUMSCHMELZE, *Differential Current Sensor for IC-CPD acc. to the standard IEC62752-2016*, October 2021.

[14] Seeed Technology, *CdS Photoconductive cell GL5528*.

[15] V. D. Benedetto, "nanoMODBUS - a compact MODBUS RTU/TCP C library for embedded/microcontrollers," https://github.com/debevv/nanoMODBUS/, April 2024, [Release: v1.17.1].